Generation of Axially Splitted Ultra-Long Multiple Optical Needles/Optical Tubes Using Generalized Cylindrical Vector Bessel Gaussian Beam Phase Modulated by Annular Walsh Function Filter

Thiruarul D.
Chikkanna Government Arts College
William Charles J.
Chikkanna government arts college
Lavanya M.
PSGR Krishnammal College for Women
Rajesh K.B (rajeskb@gmail.com)
Chikkanna Government Arts College
Jaroszewicz Z.
National Institute of Telecommunications

Research Article

Keywords: Annular Walsh function filter, Generalized CVB, Bessel Gaussian beam, SAM, energy flux density

Posted Date: March 11th, 2022

DOI: https://doi.org/10.21203/rs.3.rs-1429823/v1

Generation of axially splitted ultra-long multiple optical needles/optical tubes using generalized cylindrical vector Bessel Gaussian beam phase modulated by annular Walsh function filter

D.Thiruarul[1], J. William Charles[2], M. Lavanya[3], K.B. Rajesh[4], Z. Jaroszewicz[5]

[1,2,4]Department of Physics, Chikkanna Government Arts College, Tiruppur, Tamilnadu, India

[3]Department of Physics, PSGR Krishnammal College for Women, Coimbatore, Tamilnadu, India, 641004

[5]National Institute of Telecommunications, Szachowa 1, 04-894 Warsaw, Poland

**Corresponding author Email:rajeskb@gmail.com*

Abstract:

Based on vector diffraction theory and annular Walsh function filter, axially splitted ultra-long multiple optical needles/optical tubes of electric as well as magnetic field distributions are numerically generated by generalized cylindrical vector Bessel Gaussian beam phase modulated by annular Walsh function filter. This multiple optical structures can be conveniently tailored by properly tuning the initial phase of the Cylindrical vector beam(CVB) and Walsh order of the annular Walsh function filter. Furthermore, the effect of energy flux density(Poynting vector) as well as Spin angular momentum(SAM) distribution in the focal region are theoretically analyzed. We expect that such an axially splitted focal systems could be applicable in optical trapping and manipulation of multiple particles, optical super resolution microscopy etc.

Keywords: Annular Walsh function filter, Generalized CVB, Bessel Gaussian beam, SAM, energy flux density.

Introduction

Axially splitted sub wavelength multiple focal spots/holes with extended depth are useful for many potential application such as optical super resolution microscopy, optical trapping &manipulation of multiple particles, high density optical data storage etc[1-7]. Recently, two extreme case of generalized cylindrical vector (radial& azimuthal) beams with different types of amplitude and phase filters are used to produce the axially splitted multiple focal spots/holes. For example radially polarized beam can generates multiple focal spots by used different types of pupil plane filters[8-10]. On the other hand, an azimuthally polarized beam can generates multiple focal holes in the focal plane by using different types of pupil filters[11-14]. Except some trivial cases, synthesis & optimization of most of these pupil filters are more complicated because it has diffraction problem in general[15,16]. It is also observed that the practical implementation of this continuous varying phase filters are get tedious because they have more number of ladder step approximation. To overcoming the diffraction problems by using a set of orthogonal base function which can compute from decomposition of the pupil function. On the other hand annular Walsh function filters from annular Walsh functions overcomes the prespecified problem, by compute set of orthogonal functions as base function with finite number of discrete phase values[17]. Order of the annular Walsh filters based on three transmission values such as zero amplitude (i.e., an obstruction),unity amplitude with zero phase, unity amplitude with pi phase & size of the annular region provides an additional degree of freedom to tailoring the focal structure[18]. Hazra etal tailored the image resolution of microscopy by annular Walsh filter [19]. P. Mukherjee etal used annular filter as a pupil filter to delivered complex far-field amplitude distribution [17]. The self-similarity nature of radial,

annular, azimuthal and polar Walsh filters are studied by Hazra etal [20-23]. Recently, our group numerically generate multiple optical hole segments by tightly focused the pure azimuthally polarized beam with appropriate Walsh function filter[24]. So that, generation of axial multiple focal structures in the focal plane using annular Walsh filters as a pupil filter is altering for prespecified methods. The Poynting vector distribution and spin angular momentum (SAM) have great interest in the field of optical trapping &manipulation [25-35]. Poynting vector describes the energy in the focal region. In optical trapping &manipulation process, the SAM related to spinning of the trapped particles to it's own axis. There are so many articles demonstrate the distribution &redistribution of energy flow in the tightly focused region [36-48]. In recent years, the interaction of SAM with different type of polarizations are explotted [49-58]. In more recently, Z. Man etal analytically demonstrate the angular momentum properties of hybrid cylindrical vortex vector beam in tightly focused optical system[59,60]. In this paper, we numerically discuss the generation of axially splitted multiple focal spots/holes by tightly focusing of generalized CVB with annular Walsh function filter as a pupil filter. Furthermore, we numerically analyze the distribution of Poynting vector as well as SAM in the focal plane.

Theory

Generalized CVB:

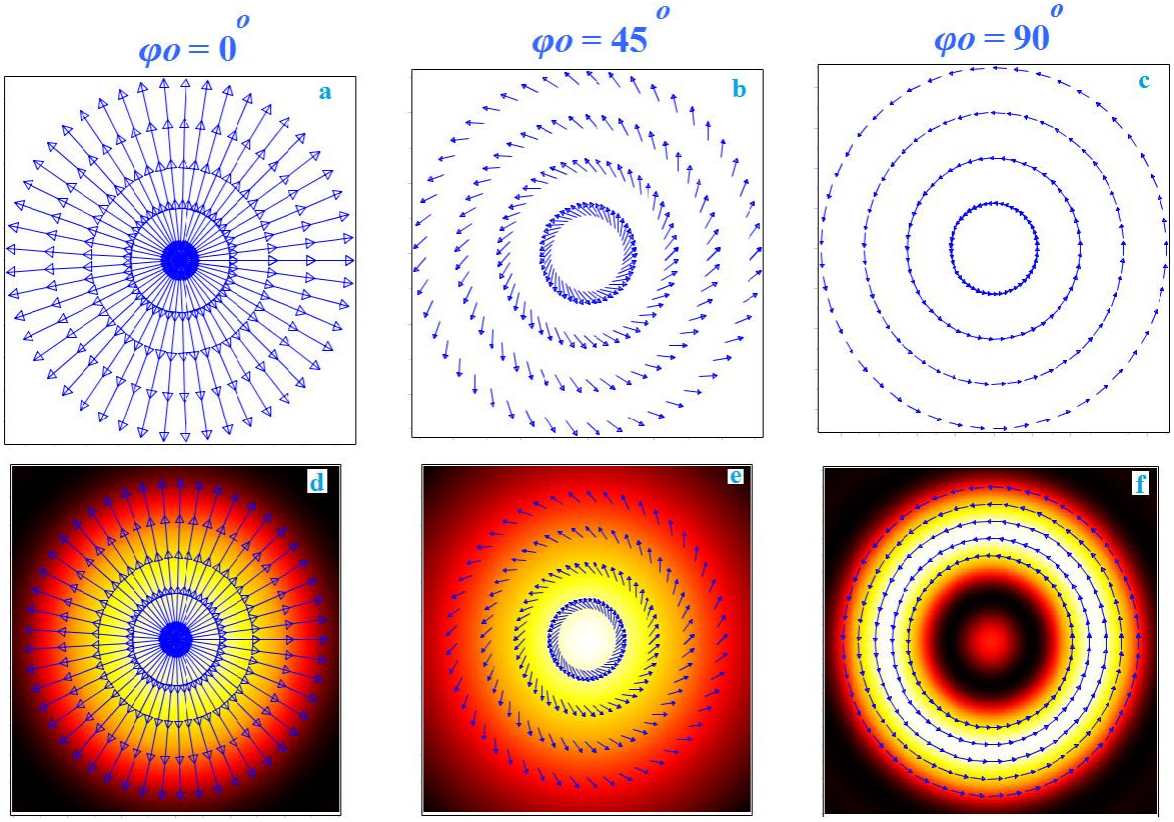

Fig.1(a-c).Polarization distribution of CVB with φ_o =0º,45º,90º.Fig.1(d-f).polarization distribution with corresponding field intensity.

The states of polarization (SoP) of the generalized cylindrical vector beam is given by[61]

$$E_0 = A_0[\cos(\phi + \varphi_0)e_x + \sin(\phi + \varphi_0)e_y]$$

Here A_0 is a constant, ϕ is the azimuthal angle, φ_o is the initial phase, e_x and e_y are unit vectors along x and y axis, respectively. The SoP only depends on the azimuthal angle $\phi(0 \leq \varphi_o \geq 2\pi)$ with their corresponding horizontal and vertical components are always in phase.Fig.1(a-c)

depicts the three kind of CVB with φ_o= 0^0,45^0,90^0.For the initial phase φ_o=0^0 and 90^0, can generates two extreme case of CVB's such as radially and azimuthally polarized beams are described in Fig.1(d &f), respectively. In-between radially and azimuthally polarized beams are called generalized CVBs for the appropriate initial phase angle φ_o.

Annular Walsh function:

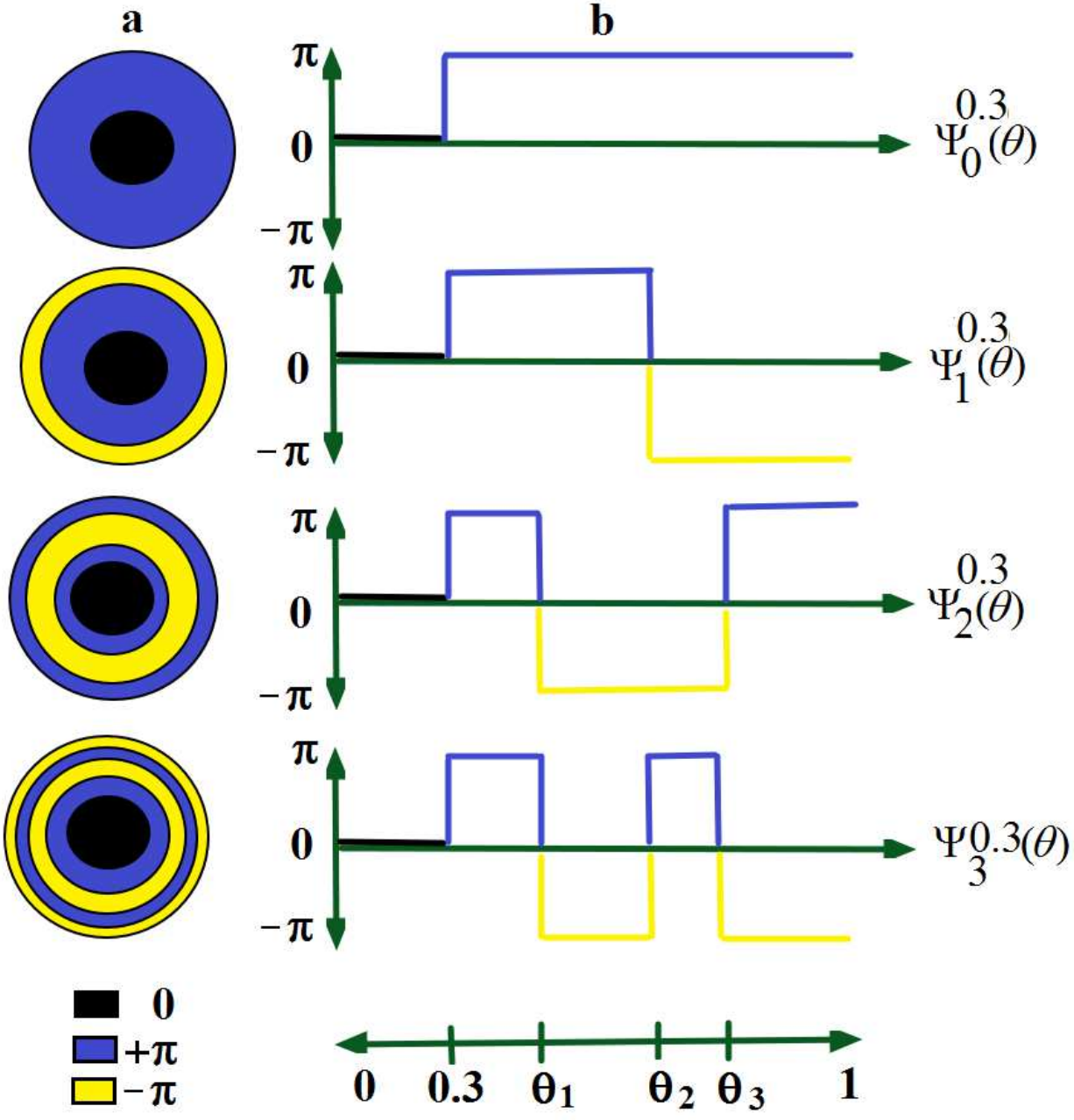

Fig.2.(a&b) Annular Walsh function $\Psi_k^{\delta}(\theta)$ ***in (θ,r) space and along θ for central annular obscuration δ=0.3,respectively.***

Walsh functions are a complete set of orthogonal functions over a given finite domain in which they take on values +1 or -1,except at a finite number of zero crossings within the domain.

Number of zero crossings within the pre-specified domain is the order of the Walsh function [17].Alike the Walsh function, annular Walsh function $\Psi_k^{\delta}(\theta)$ of index $k \geq 0$ & θ over an annular region with δ and 1 as inner and outer radii is represented in Fig.2.In fig.2, black color represents the central annular region, blue and yellow colors represents the phase transition value $+\pi$ and $-\pi$, respectively. The orthogonality conditions implies to the annular Walsh functions over the interval (δ,1) is[18]

$$\int_{\delta}^{1} \Psi_k^{\delta}(\theta)\Psi_m^{\delta}(\theta)\theta d\theta = \frac{1-\delta^2}{2}\sigma_{mn} \rightarrow (1)$$

Where

$$\sigma_{km} = \begin{cases} 0, \mathrm{k} \neq m \\ 1, \mathrm{k} = m \end{cases} \rightarrow (2)$$

σ_{km} –is the Kronecker delta.

The Walsh order k is expressed as

$$k = \sum_{m=0}^{\upsilon-1} K_m 2^m \rightarrow (3)$$

K_m are the bits,0 or 1 of the binary numerical for k, and $(2^v)$is the power of 2 that just exceeds k, for all θ in (δ,1), $\Psi_k^{\delta}(\theta)$ is defined as

$$\Psi_k^{\delta}(\theta) = \prod_{m=0}^{v-1} \mathrm{sgn}\left\{\cos\left[K_m 2^m \pi \frac{\left(\theta^2-\delta^2\right)}{\left(1-\delta^2\right)}\right]\right\} \rightarrow (4)$$

Where

$$\mathrm{sgn(y)} = \begin{cases} +1, & y > 0 \\ 0, & y = 0 \\ -1, & y < 0 \end{cases} \rightarrow (5)$$

The locations of the points of zero crossings for members of the set of functions $\Psi_k^{\delta}(\theta)$,*k=0,1,…,(M-1)* are given by

$$\theta_i = \sqrt{\frac{[(\mathrm{M}-i)]\delta^2 + i}{M}} \times \alpha \rightarrow (6)$$

The inner and outer angle of the filter is $\theta_0=\delta$ and $\theta_M=1$. α=arcsin (NA). We note that the set of *(M-1)* phase transiting(or zero crossing) locations, θ_i ,*i=1,2,…(M-1)* consist of all phase transiting locations required for specifying domains of this particular set of Walsh functions. And also an individual domain of this set of Walsh functions will have the same number of phase transition as its order.

In tight focusing condition, if the annular Walsh function presence in the input pupil, the pupil function *f(θ)* is

$$f(\theta)=\begin{cases}0, & 0\le\theta<\delta\\ \Psi_k^{\delta}(\theta), & \delta\le\theta<\alpha\end{cases}\rightarrow(7)$$

$f(\theta)$is binary (value either 0 or ± π) only in the case of zero order annular Walsh function $\Phi_0^{\delta}(\theta)$, for all other orders $f(\theta)$is ternary with (0, +π , -π).

Tight focusing of CVB with annular Walsh function filter:

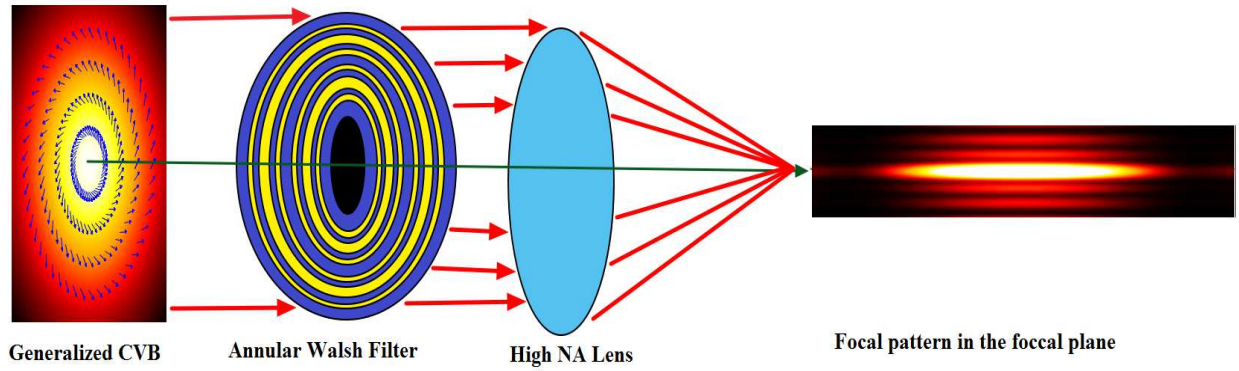

Fig.3. schematic representation for tight focusing of CVB with annular Walsh function filter.

A schematic representation for tight focusing is shown in Fig.3.Generalized cylindrical vector Bessel Gaussian beam can focus through a higher order annular Walsh function filter through a high NA lens to produce multiple axial focal structures. Based on Richards and wolf vector diffraction theory, the electric and magnetic energy densities near focal region can be derived in cylindrical coordinates *(r,ϕ,z)* as[45,61]

$$\begin{bmatrix}E_r(r,\psi,z)\\ E_\phi(r,\psi,z)\\ E_z(r,\psi,z)\end{bmatrix}=\frac{-ikf}{2\pi}\int_0^{\alpha}\int_0^{2\pi}\sin\theta\left(\sqrt{\cos\theta}\right)P(\theta)f(\theta)$$

$$\times\exp\left[ik\left(z\cos\theta+r\sin\theta\cos(\phi-\psi)\right)\right]\times\begin{bmatrix}-\sin\varphi_0\sin\phi+\cos\varphi_0\cos\theta\cos\phi\\ \sin\varphi_0\cos\phi+\cos\varphi_0\cos\theta\sin\phi\\ -\cos\varphi_0\sin\theta\end{bmatrix}d\phi d\theta\rightarrow(8)$$

$$\begin{bmatrix} H_r(r,\psi,z) \\ H_\phi(r,\psi,z) \\ H_z(r,\psi,z) \end{bmatrix} = \frac{-ikf}{2\pi} \int_0^{\alpha} \int_0^{2\pi} \sin\theta \left(\sqrt{\cos\theta} \right) \mathrm{P}(\theta) \mathrm{f}(\theta)$$

$$\times \exp\left[ik\left(z\cos\theta + r\sin\theta\cos(\phi-\psi) \right) \right] \times \begin{bmatrix} -\cos\varphi_0 \sin\phi - \sin\varphi_0 \cos\theta\cos\phi \\ \cos\varphi_0\cos\phi - \sin\varphi_0\cos\theta\sin\phi \\ -\sin\varphi_0\sin\theta \end{bmatrix} d\phi d\theta \rightarrow (9)$$

Here α=arcsin(NA/n) is maximum tangential angle of the high NA lens.*NA* represents the numerical aperture of the objective lens. *n* denotes the refractive index of the surrounding medium. $k=2\pi/\lambda$ is the wave number in free space and *f* is the focal distance. *P(θ)*is the relative amplitude of the input Bessel Gaussian beam at the entrance pupil is given by[45,61]

$$\mathrm{P}(\theta) = \exp\left[-\beta_0{}^2 \left(\frac{\sin(\theta)}{\sin\alpha} \right)^2 \right] J_1\left(2\beta_0 \frac{\sin(\theta)}{\sin\alpha} \right) \rightarrow (10)$$

Where β_0 is a beam parameter indicates the ratio between pupil diameters to beam diameter.$J_1(x)$ is the first order Bessel function. If the annular Walsh function filter is placed at the pupil plane, the pupil function *P(θ)* is replacing by *P(θ)f(θ).*

The Spin-angular momentum (SAM) density or an arbitrary time-harmonic beam is defined as[59]

$$S = \left(\frac{\mathrm{Im}[\varepsilon_0(E^* \times E) + \mu_0(H^* \times H)]}{4\omega} \right) \rightarrow (11)$$

Where ω is the angular frequency of the laser beam.* denotes the complex conjugate and *Im[x]* denotes the imaginary value of the *x*.ε_0 and μ_0 are the vacuum permittivity and permeability. The interaction between magnetic field and particle is weaker than the interaction between electric field and particle. So that, the SAM interms of electric field is given by

$$\left.\begin{aligned} S_r &= \frac{\varepsilon_0}{4\omega} \mathrm{Im}(E_\phi^* E_z - E_\phi E_z^*) \\ S_\phi &= \frac{\varepsilon_0}{4\omega} \mathrm{Im}(E_z^* E_r - E_z E_r^*) \\ S_z &= \frac{\varepsilon_0}{4\omega} \mathrm{Im}(E_r^* E_\phi - E_r E_\phi^*) \end{aligned}\right\} \rightarrow (12)$$

In terms of the electric and magnetic fields, the time averaged Poynting vector *P* in cylindrical coordinates is given by[36]

$$\left.\begin{aligned} P_r &= \left(\frac{c}{8\pi}\right)\mathrm{Re}\left(E_\phi M_z^* - E_z M_\phi^*\right) \\ P_\phi &= \left(\frac{c}{8\pi}\right)\mathrm{Re}\left(E_z M_r^* - E_r M_z^*\right) \\ P_z &= \left(\frac{c}{8\pi}\right)\mathrm{Re}\left(E_r M_\phi^* - E_\phi M_r^*\right) \end{aligned}\right\} \rightarrow (13)$$

Where c denotes velocity of light and the asterisk means the complex conjugation. *Re[x]* denotes the real value of x. The other numerical values are $\lambda=1$, $n=1$,$k=2\pi/\lambda$, $NA=0.85$,$\alpha=\arcsin(NA)$.

Result and discussion:

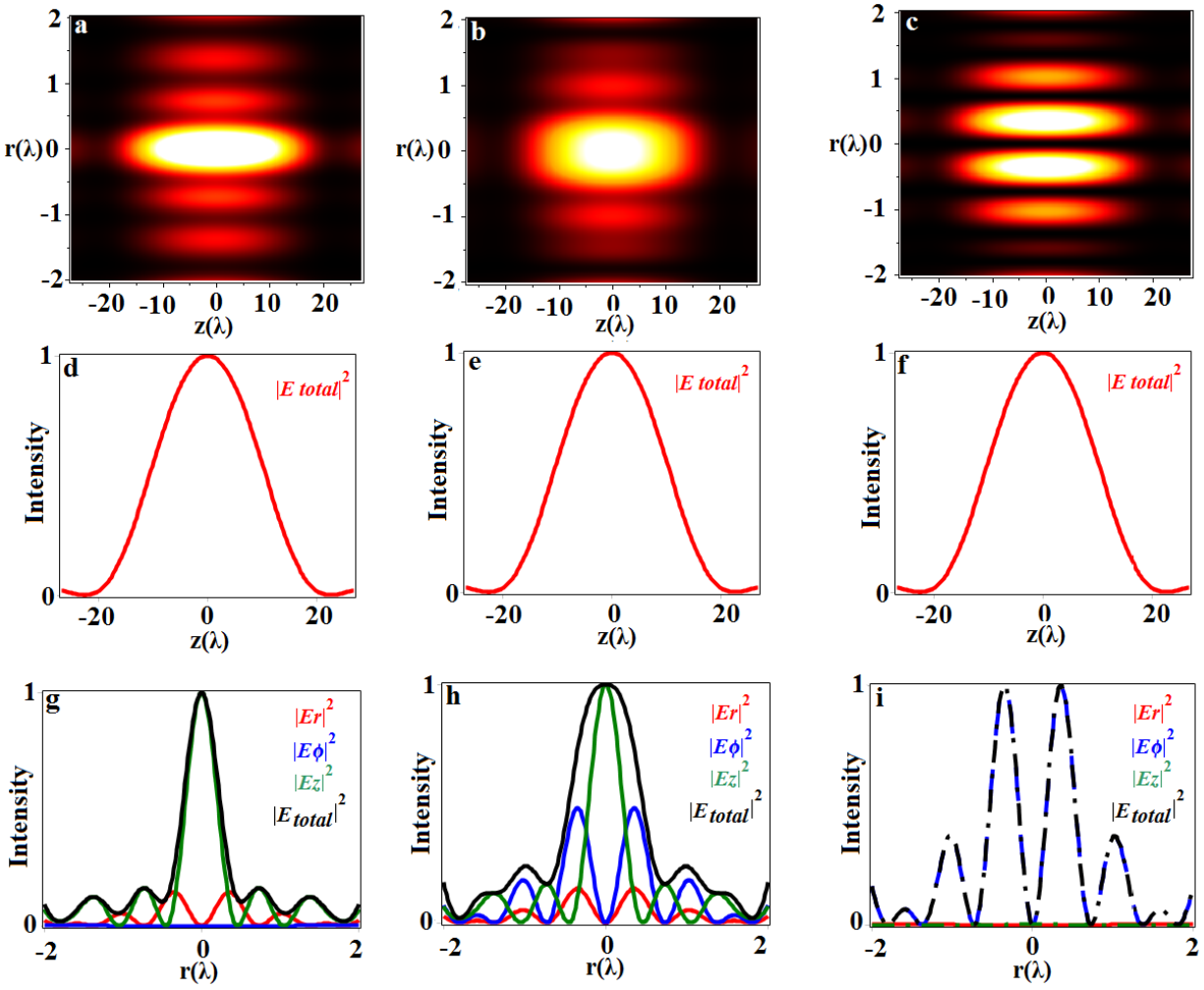

Fig.4. Calculated electric energy density in the focal region for initial phase φ_o =0⁰,45⁰,90⁰ with Walsh order k=2, annular obstruction δ=0.9 with β=1.2.Fig.4.(a-c),(d-f),(g-i) describes the 2D surface distribution of $|E|^2$ in r-z plane and their corresponding axial and radial intensity distributions, respectively.

Fig.4. shows the electric field distribution for three kinds of CVBs in the focal plane. Initial phase angle φ_o as 0^0 with Walsh order $k=2$ and annular obstruction δ as 0.9,can generates an ultra long optical needle as depicted in Fig.4.(a) and the their corresponding axial and radial intensity distributions are mentioned in Fig.4.(d) and (g),respectively. From fig.4.(d & g), the generated

optical needle have FWHM(Full Width Half Maximum) of ~0.37λ and DOF(Depth of Focus) of ~14.47λ. tuning the initial phase angle from 0^0 to 45^0,the focal structure can be broadened in radial direction as shown in Fig.4.(b,e,h). from fig.4.(h), the total electric field component can be dominated by peak centered E_z component as well as annular shaped E_ϕ component. Further increasing φ_o as 90^0,an ultra long optical tube can generated with FWHM of ~0.37λ and DOF of ~14.47λ as depicted in Fig.4.(c,f,i).The total electric field can only dominated by E_ϕ component(from fig.4.(i). We concluded from above result, one can generates both ultra long optical needle as well as optical tube for special case of generalized CVBs such as radial($\varphi_o=0^0$) and azimuthal($\varphi_o=90^0$) beams. Moreover, the FWHM and DOF achieved here is much higher than the our previously proposed methods .[62-64] These focal structures found potential applications in optical recording, optical trapping, optical microscopy etc[1-7].

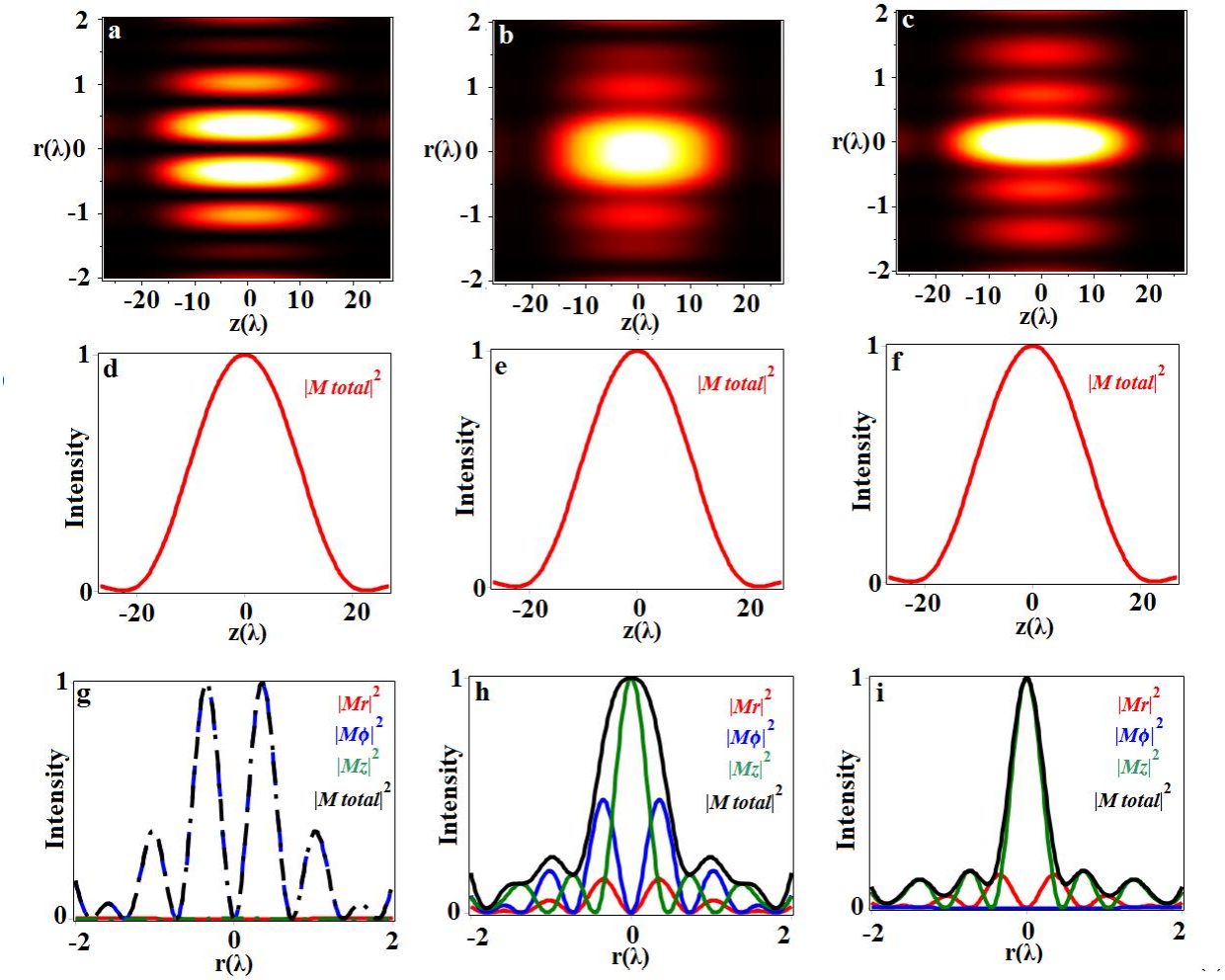

Fig.5. Calculated magnetic energy density in the focal region for initial phase $\varphi_o=0^0,45^0,90^0$ with Walsh order k=2, annular obstruction δ=0.9 with β=1.2.Fig.4.(a-c),(d-f),(g-i) describes the 2D surface distribution of $|M|^2$ in r-z plane and their corresponding axial and radial intensity distributions, respectively.

Fig.5. shows the magnetic field distribution in the focal plane. The parameters are same as in fig.4. For radially polarized beam ($\varphi_o=0^0$), can generates an ultra long optical tube, dominated only by M_ϕ component as depicted in Fig.5.(a,d,g). For initial angle φ_o as 45^0,the magnetic field

distribution is same like as electric field distribution as shown in Fig.5.(b,e,h).For an azimuthally polarized beam($\varphi_o=90^0$),the magnetic field turns to an ultra long magnetic needle, dominated by only M_z component as shown in Fig.5.(c,f,i). The FWHM and DOF values of generated magnetic field distributions are same as in electric field distribution. The generated ultra long magnetic needle and tube can have application in magnetic recording, magnetic resonance microscopy etc[65-67].

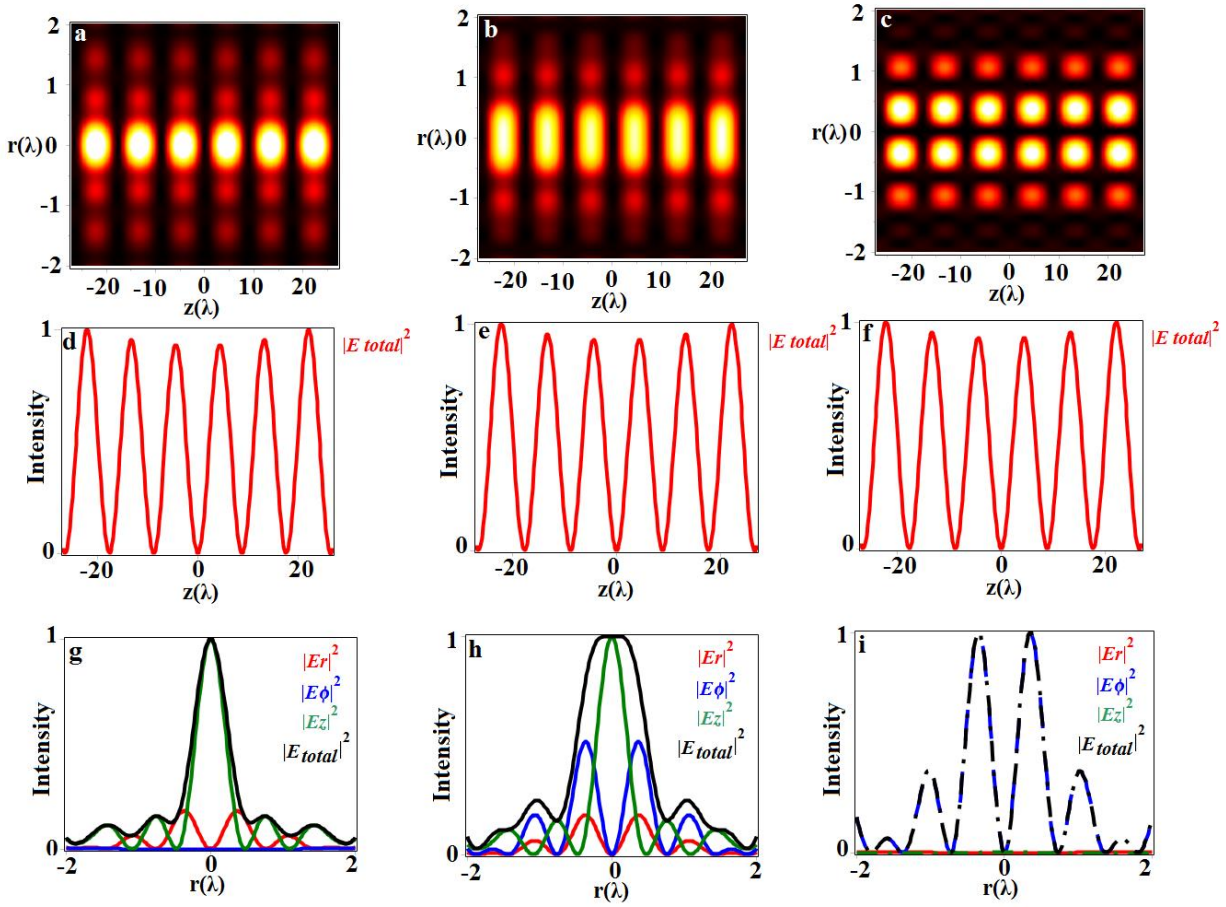

Fig.6. Calculated electric energy density in the focal region for initial phase φ_o =0^0,45^0,90^0 with Walsh order k=25, annular obstruction δ=0.9 with β=1.2.Fig.4.(a-c),(d-f),(g-i) describes the 2D surface distribution of $|E|^2$ in r-z plane and their corresponding axial and radial intensity distributions, respectively.

Fig.6. as same like as Fig.4. but for *k* as 25.For higher Walsh order(*k=25*),can generates axially splited, co-axially equidistant self similar multiple optical needles and optical tubes in the geometrical plane. The radially polarized CVB($\varphi_o=0^0$) with higher Walsh order(*k=25*) can generates an optical segment with six self similar optical needles in the range of -25λ to 25λ along the optical axis. Each optical needle have FWHM of ~0.34λ,DOF of ~4.36λ and distance between them are measured as ~4.4λ.further increasing φ_o as 45^0 ,can generates an optical segment which contains six radial flattop profiled optical needles With FWHM of ~0.55λ and DOF of ~4.36λ as shown in Fig.6.(b,e,h).On the other hand, an azimuthally polarized CVB($\varphi_o=90^0$) can created an focal segment with six self similar, axially splited optical tubes in the focal region as shown in Fig.6.(c,f,i).The values such as FWHM and DOF are same like as

values of optical needles in the optical segment for radially polarized beam. These multiple optical needles and optical tubes have potential applications in multiple optical trapping and recording, multiple optical manipulation, high resolution microscopy etc[1-7].

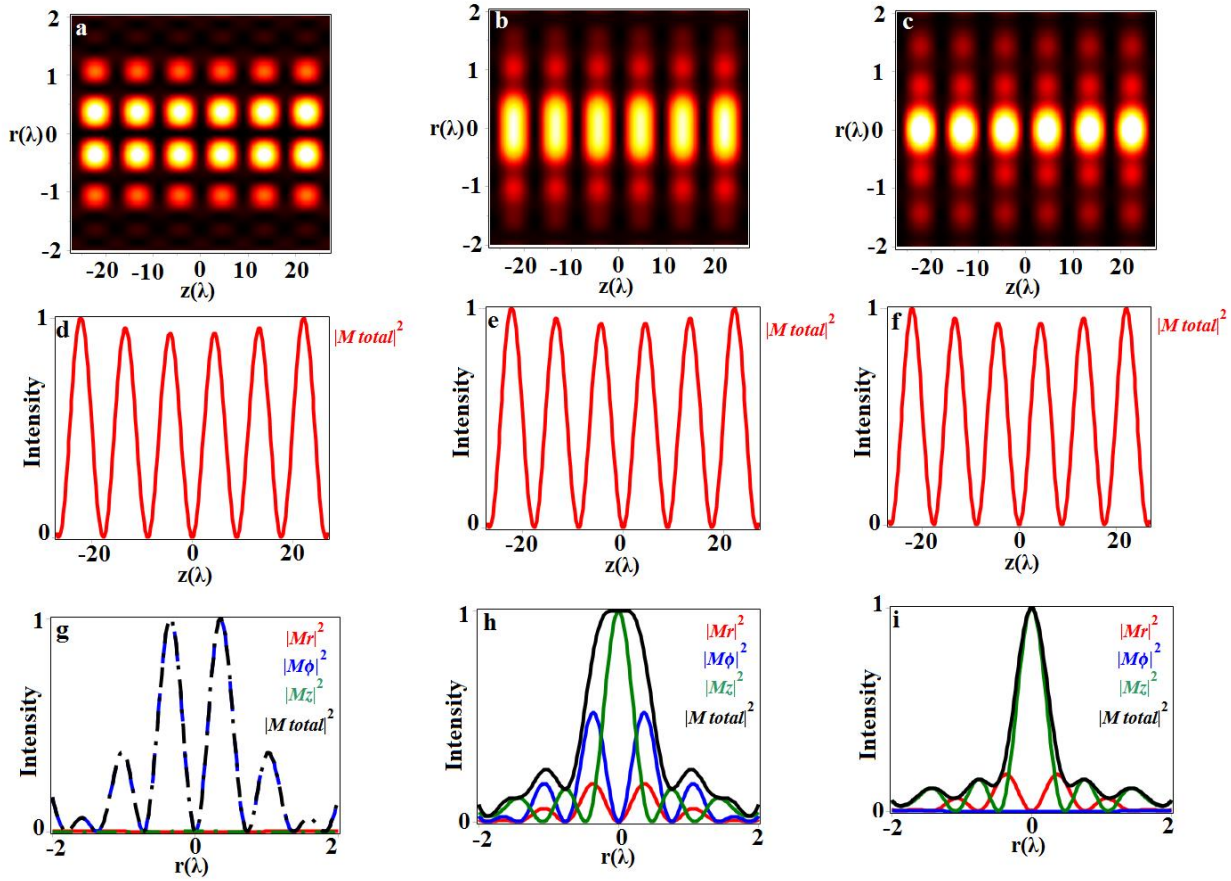

Fig.7. Calculated magnetic energy density in the focal region for initial phase φ_o =0^0,45^0,90^0 with Walsh order k=25, annular obstruction δ=0.9 with β=1.2.Fig.4.(a-c),(d-f),(g-i) describes the 2D surface distribution of $|M|^2$ in r-z plane and their corresponding axial and radial intensity distributions, respectively.

On the other hand, higher Walsh order(*k=25*) for magnetic field, can generates magnetic tube segment as well as magnetic needle segment for radially and azimuthally polarized CVBs, respectively. The number of focal structures in the segment and size of them are same as in Fig.6.This multiple magnetic needles and magnetic tubes can increase the performance of magnetic recording ,magnetic resonance microscopy etc[65-67].

Overall, the initial phase angle of the generalized CVB can change the focal pattern from focal spot to focal hole (in electric field distribution) or focal hole to focal spot (in the magnetic field distribution). Similarly, increasing the Walsh order(*k>2*) with high annular value can split the focal structures in the axial plane with long focal depth. The overall values of FWHM and DOF are summarized in table 1.

Focal Structures	**Walsh order k**	**Annular Obstruction δ**	**Beam parameter β**	**FWHM(λ)**	**DOF(λ)**

Electric/magnetic needle of spot	2	0.9	2	0.37	14.47
Electric/magnetic needle of hole	2	0.9	2	0.37	14.47
Electric/magnetic multiple spots	25	0.9	1.2	0.34	4.36
Electric/magnetic multiple holes	25	0.9	1.2	0.34	4.36

Table .1.FWHM & DOF values for generated focal structures.

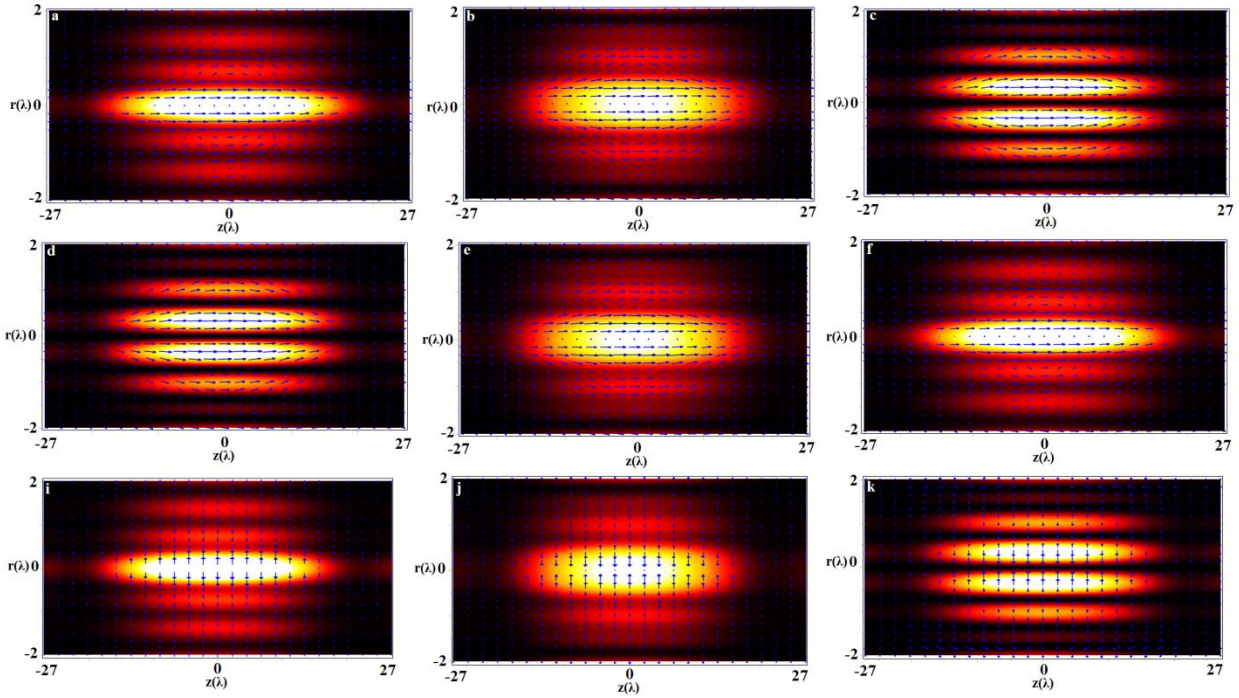

Fig.8.(a-c) and (d-f) shows the distribution of energy flux density on the electric and magnetic field for k=2,δ=0.9,β=2.(i-k) shows the SAM density on the electric field distribution.

In Fig.8 (a-c), (d-f) & (i-k) , we numerically studied the distribution of the Poynting vector(energy flow) on the electric field, magnetic field and as well as SAM density on the electric field, respectively. The black arrow marks remains the energy flow in Fig.8 (a-c & d-f) and SAM flow in fig.8 (i-k). From Fig(a-c, d-f), we noted that the strong forwarded longitudinal energy flow occurred above and below the radial axial for electric as well as magnetic fields corresponding to the initial phase angle values 0^0,45^0,90^0. At initial phase angle $\varphi_o=0^0$, SAM flow is outward from the optic axis. Further increase initial angle from 0^0 to 45^0 and 90^0, SAM flows to inward towards the optic axis. From Fig.8.we conclude that their is no energy flows as well as SAM flows at the centre of the optic axis.

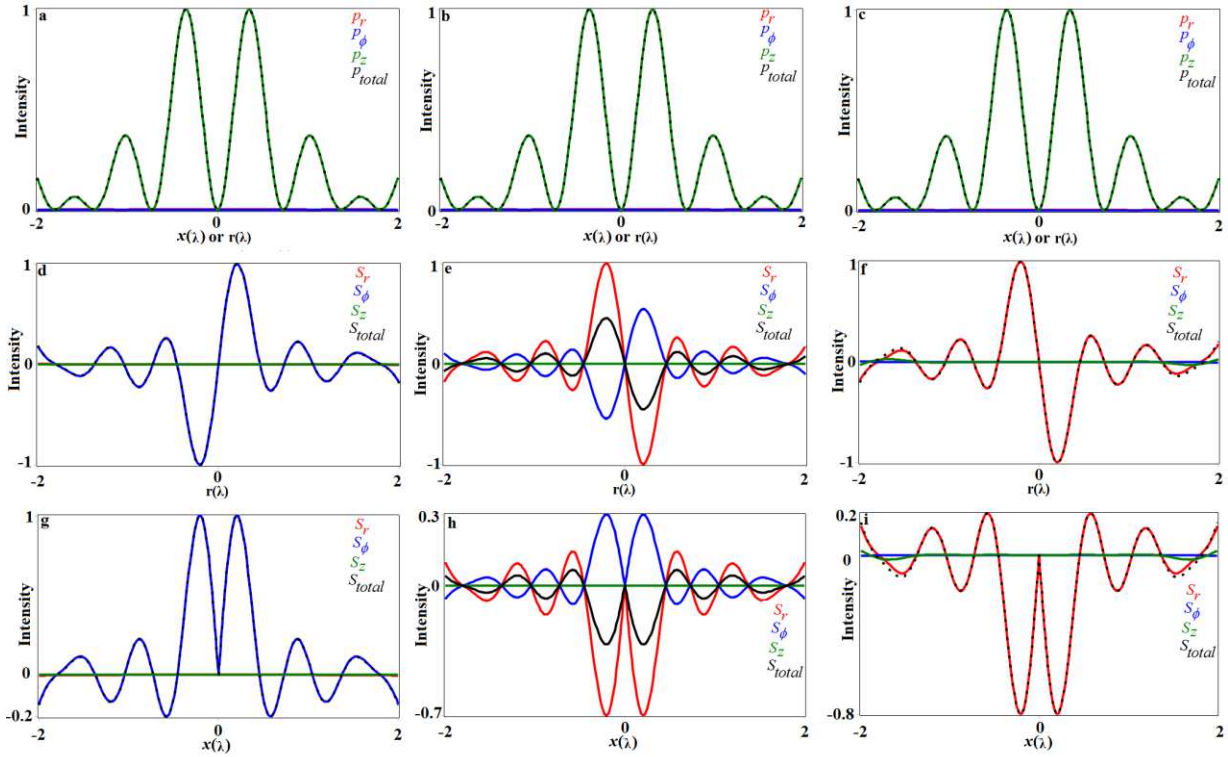

Fig.9.(a-c) shows the distribution of 1D energy flux density in r plane(z=0) or in x plane ($z=0, r=(x^2+y^2)^{1/2}, y=0$) with $k=2, \delta=0.9, \beta=2$ for $\varphi_o = 0^0, 45^0, 90^0$.(d-f) & (g-i) shows the SAM density in r and x plane, respectively.

Fig.9. shows the 1D energy flow and SAM flow in both *r* & *x* plane. By compare, fig.8.(a-f) with fig.9.(a-c), energy flow is forward donut shaped for both electric and magnetic fields in *x* and *r* plane. However, SAM flow is changing for each value of initial phase angle φ_o. To compare fig.8.(i) with fig.9(g),the SAM flow is forward donut shaped with only domination of S_ϕ component .After increasing the φ_o *to* 45^0, SAM turns to reversed with presence of both S_r and S_ϕ components is shown in Fig.9.(h). Further increasing φ_o to 90^0, the donut shaped SAM intensified in the reverse direction with only presence of radial component S_r (from fig.9(i)).

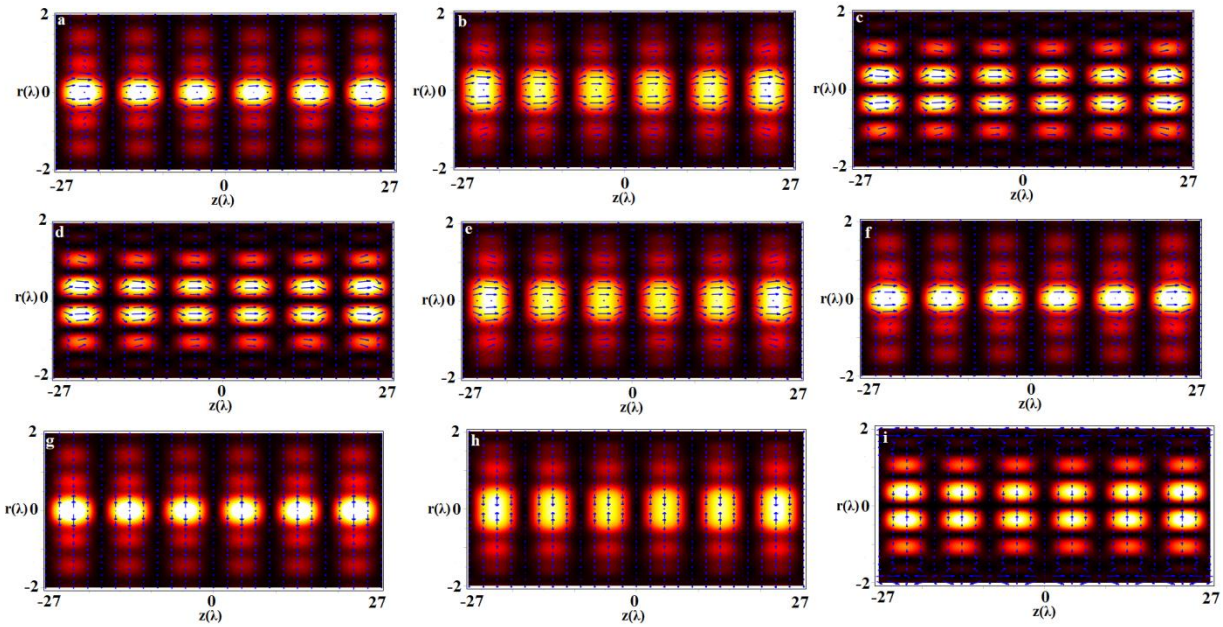

Fig.10.(a-c) and (d-f) shows the distribution of energy flux density on the electric and magnetic field for k=25,δ=0.9,β=1.2.Fig.9.(g-i) shows the SAM density on the electric field distribution.

Fig.10. is same as in fig.8. but for Walsh order *k=25* and beam parameter *β=1.2*.For the effect of higher Walsh order, the single focal structure can splitted into multiple number of self-similar focal structures. However there is no changes in the energy flow as well as SAM flow is shown in fig.10 (to compare fig.8). So that, higher Walsh order cannot affects the energy as well as SAM distribution in the focal plane. These findings can useful in multiple optical trapping and manipulation.

Conclusion:

The effect of annular Walsh function filter for generation of axially splitted ultra-long multiple optical needles/optical tubes of electric as well as magnetic field distributions are numerically studied based on the vector diffraction theory. For lower Walsh order can generates single axially extended focal patterns corresponding to initial phase angle of the generalized cylindrical vector Bessel Gaussian beam. On the other hand, for higher Walsh order with appropriate initial cylindrical angle to generates axially splitted self-similar multiple ultra long optical structures. The distribution properties of Poynting vector as well as SAM densities in the focal region are theoretically demonstrated. We conclude that, such an axially splitted focal systems could be applicable in optical trapping and manipulation of multiple particles, optical microscopy etc.

Acknowledgments:
The authors would like to thank **Dr. L.N. Hazra**(University of Calcutta, Kolkata, India) for his motivational and suggestions to carry out this work. This work is supported by the Department of Science and Technology (DST), India, under project SERB-YSS (F.No. 2015/001852).

Reference

1. Bingen, P., Reuss, M., Engelhardt, J., and Hell, S.W.: Parallelized STED fluorescence nanoscopy. Opt. Express **19,**23716-23726(2011). https://doi.org/10.1364/OE.19.023716.
2. Rong, Z., Kuang, C., Fang, Y., Zhao, G., Xu, Y.& X. Liu.: Super-resolution microscopy based on fluorescence emission difference of cylindrical vector beams. Opt. Commun. **354** ,71–78(2015) . https://doi.org/10.1016/j.optcom.2015.05.057.
3. Yehoshua, S., Pollari,R., & Milstein, J. N.: Axial Optical Traps: A New Direction for Optical Tweezers. Biophys. J.**108**,2759-2766(2015) . https://doi.org/10.1016/j.bpj.2015.05.014.
4. Liang, Y., Yan, S., Wang, Z., Li, R., Cai, Y., He, M., , … Lei, M.:Simultaneous optical trapping and imaging in the axial plane: a review of current progress. Rep. Prog. Phys. (2020). doi:10.1088/1361-6633/ab7175.
5. Fuxi, G., Yang, W.: Data storage at the nano scale. Boca Raton: CRC Press, Taylor & Francis. 2015. p. 26–28. https://doi.org/10.1201/b18094.
6. Li, X., Cao, Y., Tian, N., Fu, L., and Gu, M.: Multifocal optical nanoscopy for big data recording at 30 TB capacity and gigabits/second data rate. Optica **2**, 567-570(2015). https://doi.org/10.1364/OPTICA.2.000567.
7. Ren, H., Lin, H., Li, X., and Gu, M.: Three-dimensional parallel recording with a Debye diffraction-limited and aberration-free volumetric multifocal array. Opt. Lett. **39,** 1621-1624(2014).https://doi.org/10.1364/OL.39.001621.
8. Yu, Y., Zhan, Q.: Creation of identical multiple focal spots with prescribed axial distribution. Sci Rep **5**, 14673 (2015).https://doi.org/10.1038/srep14673.
9. Wang, X., Gong, L., Zhu, Z., Gu, B., and Zhan Q.: Creation of identical multiple focal spots with three-dimensional arbitrary shifting. Opt. Express **25**, 17737-17745(2017).
10. Prabakaran, K., Rajesh, K.B., Pillai, T. V. S., Chandrasekaran, R.& Sarasvathi, R. C.: Generation of multiple focal spot using phase modulated radially polarized TEM11 * mode beam. Journal of Optics, **44**(4), 311–316(2015). doi:10.1007/s12596-015-0309-y.
11. Guo, H., Weng, X., Jiang, M., Zhao, Y., Sui, G., Hu, Q., Wang, Y., and Zhuang, S.:Tight focusing of a higher-order radially polarized beam transmitting through multi-zone binary phase pupil filters. Opt. Express **21**(5), 5363– 5372(2013). https://doi.org/10.1364/OE.21.005363.
12. Yu, Y., Huang, H., Zhou, M., Zhan, Q.:Engineering of multi-segmented light tunnel and flattop focus with designed axial lengths and gaps. Opt. Commun. **407**,398–401(2018).doi:10.1016/j.optcom.2017.09.075.
13. Chandrasekaran, R., Prabakaran, K., Rajesh, K.B.: Generation of multiple focal spot and focal hole segments using phase modulated cylindrically polarized annular multi-Gaussian beam. Opt Quant Electron **48**,1-9(2016). DOI: 10.1007/s11082-015-0311-2.
14. Lalithambigai, K., Anbarasan, P. M., Rajesh, K. B.:Creation of super-length optical tube by phase modulated azimuthally polarized beam with multi-zone phase filter. Optik, 126(5), 554–557(2015). doi:10.1016/j.ijleo.2015.02.009.
15. Prabakaran, K., Rajesh, K.B. & Pillai T.V.S.: Generation of multiple sub wavelength focal hole segments using azimuthally polarized hollow Gaussian beam. Opt Quant Electron **47**,1283–1289(2015). DOI: 10.1007/s11082-014-9990-3.

16. Gould, T. J., Burke, D., Bewersdorf, J., Booth, M. J.: Adaptive optics enables 3D STED microscopy in aberrating specimens. Optics Express, **20**(19), 20998-21009(2012).https://doi.org/10.1364/OE.20.020998.
17. Hao, X., Antonello, J., Allgeyer, E. S., Bewersdorf, J., Booth, M. J.: Aberrations in 4Pi Microscopy. Optics Express, **25**(13),14049-14058. (2017) https://doi.org/10.1364/OE.25.014049.
18. Walsh, J.L.: A closed set of normal orthogonal functions. Am. J. Math.**45**, 5–24. (1923)
19. Mukherjee, P., Hazra, L. N., Far field diffraction properties of annular Walsh filters. Adv. Opt. Technol. **2013**,360450(2013). https://doi.org/10.1155/2013/360450.
20. Hazra, L.N., Walsh filters in tailoring of resolution in microscopic imaging. Micron **38,** 129–135(2007). doi:10.1016/j.micron.2006.07.003.
21. Mukherjee, P., Hazra, L.N.: Self-similarity in radial Walsh filters and axial intensity distribution in the far field diffraction pattern. J Opt Soc Am A **31**(2), 379–387(2014) .https://doi.org/10.1364/JOSAA.31.000379.
22. Mukherjee, P., Hazra, L.N.: Self-similarity in the far field diffraction patterns of annular Walsh filters. Asian J. Phys.**23**(4), 543–560(2014).
23. Mukherjee, P., Hazra, L.N.: Self-similarity in transverse intensity distributions in the far field diffraction pattern of radial Walsh filters. Adv. Opt.**2014**,7(2014) . https://doi.org/10.1155/2014/352316
24. Thiruarul, D., Rajesh, K.B., Lavanya, M.: Generation of ultra-long multiple optical tubes using annular Walsh function filters, Opt Quant Electron **52**, 9 (2020)1-14. DOI: 10.1007/s11082-020-02507-1.
25. Litvin, I. A., Dudley, A., and Forbes, A.: Poynting vector and orbital angular momentum density of super positions of Bessel beams. Opt. Express **19**,16760-16771(2011). https://doi.org/10.1364/OE.19.016760.
26. Sztul, H.I., Alfano, R.R.: The Poynting vector and angular momentum of Airy beams, Opt. Express **16**, 9411-9416 (2008).https://doi.org/10.1364/OE.16.009411
27. Bergman, J E S et al 2008 Conservation laws in generalized Riemann–Silberstein electrodynamics arXiv:0803.2383v6
28. Tang, Y. and Cohen, A .E .:Optical chirality and its interaction with matter Phys. Rev. Lett. **104**, 163901(2010). https://doi.org/10.1103/PhysRevLett.104.163901.
29. Hendry, E., Carpy, T., Johnston, J., et al. Ultrasensitive detection and characterization of biomolecules using superchiral fields. Nature Nanotech **5**, 783–787(2010). https://doi.org/10.1038/nnano.2010.209.
30. Bliokh, K., Nori, F.: Characterizing optical chirality. Phys. Rev. A **83** ,021803(2011) (R). doi:10.1103/physreva.83.021803
31. Shi, Y., Zhu, T., Zhang, T., et al. Chirality-assisted lateral momentum transfer for bidirectional enantioselective separation. Light Sci Appl **9,** 62 ,1-12(2020). https://doi.org/10.1038/s41377-020-0293-0
32. Angelsky, O. V., Bekshaev, A. Y., Maksimyak, P. P., Maksimyak, A. P., Hanson, S. G. & Zenkova, C. Y.: Orbital rotation without orbital angular momentum: mechanical action of the spin part of the internal energy flow in light beams. Opt. Express, **20**(4), 3563-71(2012).DOI: 10.1364/OE.20.003563.
33. Pan, Y., Gao, X.-Z., Zhang, G.-L., Li, Y., Tu, C.& Wang, H.-T., Spin angular momentum density and transverse energy flow of tightly focused kaleidoscope-structured vector optical fields. APL Photonics, **4**(9), 096102(2019). doi:10.1063/1.5117269.

34. Allen, L., Barnett, S.M., Padgett ,M.J.:2003 Optical Angular Momentum (Bristol: Institute of Physics)
35. Yao, A .M. and Padgett, M. J.: Orbital angular momentum: origins, behavior and applications. Adv. Opt. Photonics **3** 161–204(2011). https://doi.org/10.1364/AOP.3.000161.
36. Andrews, D .L, Babiker, M. (2013). The Angular Momentum of Light (Cambridge: Cambridge University Press).
37. Man, Z., Bai, Z., Zhang, S., Li, X., Li, J., Ge, X., Zhang, Y., Fu, S.:Redistributing the energy flow of a tightly focused radially polarized optical field by designing phase masks. Opt. Express **26**,23935-23944(2018).DOI: 10.1364/OE.26.023935.
38. Gaffar, M., Boruah, B. R.: Poynting vector profile of a tightly focused radially polarized beam in the presence of primary aberrations. J. Opt. Soc. Am. A 32 660-668(2015).DOI: 10.1364/JOSAA.32.000660.
39. Jiao, X., Liu, S., Wang, Q., Gan, X., Li, P., Zhao, J.: Redistributing energy flow and polarization of a focused azimuthally polarized beam with rotationally symmetric sector-shaped obstacles. Opt. Lett. **37**(6), 1041–1043(2012). DOI: 10.1364/OL.37.001041
40. Yuan, G. H., Wei, S. B., Yuan X. C.: Generation of non-diffracting quasi-circular polarization beams using an amplitude modulated phase hologram.J. Opt. Soc. Am. A **28**(8) ,1716–1720(2011). DOI: 10.1364/JOSAA.28.001716.
41. Zhang ,Y., Ding, B.:Magnetic field distribution of a highly focused radially-polarized light beam. Opt. Express **17**, 22235–22239(2009). doi: 10.1364/OE.17.022235.
42. Wu, G., Wang, F., Cai, Y.: Generation and self-healing of a radially polarized Bessel–Gauss beam. Phys. Rev. A **89**, 043807 (2014).DOI: 10.1103/PhysRevA.89.043807.
43. Gao, X.-Z., Pan, Y., Zhang, G.-L., Zhao, M.-D., Ren, Z.-C.,. Tu, C.-G, Li, Y.-N., and Wang, H.-T.: Redistributing the energy flow of tightly focused ellipticity-variant vector optical fields, Photon. Res. **5**(6),640–648(2017). doi:10.1364/prj.5.000640.
44. Man, Z., Li, X., Zhang, S., Bai, Z., Lyu, Y., Li, J., Fu, S.: Manipulation of the transverse energy flow of azimuthally polarized beam in tight focusing system. Opt. Commun. **431**,174-180(2018). doi:10.1016/j.optcom.2018.09.028.
45. Richards, B., and Wolf, E.:Electromagnetic diffraction in optical systems, ii. structure of the image field in an aplanatic system. Proc. R. Soc. Lond. A **253**(1274), 358–379(1959). https://doi.org/10.1098/rspa.1959.0200.
46. Kotlyar, V.V., Stafeev, S.S., Kovalev, A. A.: Reverse and toroidal flux of light fields with both phase and polarization higher-order singularities in the sharp focus area.Opt. Express **27** (12),16689-16702(2019).https://doi.org/10.1364/OE.27.016689.
47. Stafeev, S.S., Kotlyar, V.V, Nalimov, A.G., Kozlova, E.S.:The non-vortex inverse propagation of energy in a tightly focused high-order cylindrical vector beam. IEEE Photonics Journal **11** (4) ,1-10(2019).DOI: 10.1109/JPHOT.2019.2921669.
48. Stafeev, S.S., Kotlyar, V.V.: Elongation of the area of energy backflow through the use of ring apertures. Opt. Commun.**450**, 67-71(2019).DOI: 10.1016/j.optcom.2019.05.057
49. Zhao, Y .Q., Edgar, J .S., Jeffries, G .D. M ., McGloin, D., Chiu, D. T.: Spin-to-orbital angular momentum conversion in a strongly focused optical beam .Phys. Rev. Lett. **99**, 073901(2007).doi: 10.1103/PhysRevLett.99.073901.
50. Monteiro, P. B., Neto, P.A.M., Nussenzveig, H.M .: Angular momentum of focused beams: Beyond the paraxial approximation. Phys. Rev. A **79**,033830(2009). doi:10.1103/PhysRevA.79.033830.

51. Prajapati. C.: Study of electric field vector, angular momentum conservation and Poynting vector of non paraxial beams. J. Opt. **23**,025604(2021) . https://doi.org/10.1088/2040-8986/abe1cc.
52. Han, L., Liu, S., Li, P., Zhang, Y., Cheng, H.C., Zhao, J.L.: Catalystlike effect of orbital angular momentum on the conversion of transverse to three-dimensional spin states within tightly focused radially polarized beams. Phys. Rev. A **97**,053802(2018). https://doi.org/10.1103/PhysRevA.97.053802.
53. Shu, J., Pu, J. and Liu, Y.:Angular momentum conversion of elliptically polarized beams focused by high numerical-aperture phase Fresnel zone plates. Appl. Phys. B **104**, 639-646(2011). https://doi.org/10.1007/s00340-011-4454-y.
54. Zhu, W ., Shvedov, V., She, W., Krolikowski, W.: Transverse spin angular momentum of tightly focused full Poincaré beams. Opt. Express **23,** 34029 (2015)https://doi.org/10.1364/OE.23.034029.
55. Bomzon, Z., Gu, M., Shamir, J.: Angular momentum and geometrical phases in tight-focused circularly polarized plane waves Appl. Phys. Lett. **89**, 241104(2006).DOI: 10.1063/1.2402909.
56. Chen, L.X., She, W.L.: Electro-optically forbidden or enhanced spin-to-orbital angular momentum conversion in a focused light beam. Opt. Lett. **33**,696-698(2008). https://doi.org/10.1364/OL.33.000696.
57. Zhang ,Y. D., Xue, Y.X., Zhu, Z.Q., Rui, G. H., Cui, Y. P., Gu, B.: Theoretical investigation on asymmetrical spinning and orbiting motions of particles in a tightly focused power-exponent azimuthal-variant vector field. Opt. Express **26,** 4318-4329(2018). https://doi.org/10.1364/OE.26.004318.
58. Bliokh, K .Y., Bekshaev, A. Y., Nori, F.:Optical momentum, spin, and angular momentum in dispersive media Phys. Rev. Lett. **119** ,073901(2017). DOI: 10.1103/PhysRevLett.119.073901.
59. Meng, P., Man, Z., Konijnenberg, A. P., and Urbach, H. P.: Angular momentum properties of hybrid cylindrical vector vortex beams in tightly focused optical systems. Opt. Express **27**, 35336-35348(2019).https://doi.org/10.1364/OE.27.035336.
60. Man, Z., Dou, X., Urbach, H. P.: The evolutions of spin density and energy flux of strongly focused standard full Poincaré beams. Opt. Commun. **458**,124790(2020). DOI: 10.1016/j.optcom.2019.124790.
61. Youngworth, K. S., Brown, T. G.: Focusing of high numerical aperture cylindrical-vector beams, Opt. Express **7**(2),77–87(2000). https://doi.org/10.1364/OE.7.000077.
62. Seethalakshmi, S., Udhayakumar, M., Priyadharsini, N., et al.: Generation of sub-wavelength longitudinal magnetic probe and multiple spots using circularly polarized annular multi-Gaussian beam. J Opt **48**,586–593(2019). https://doi.org/10.1007/s12596-019-00571-9.
63. Senthilkumar, M., Rajesh, K.B., Udhayakumar, M., Jaroszewicz, Z., Mahadevan, G.: Focusing properties of spirally polarized sinh Gaussian beam. Optics & Laser Technology, **111**,623–628(2019). doi:10.1016/j.optlastec.2018.10.048.
64. Chandrasekaran, R., Prabakaran, K., Rajesh, K.B., Ravi, V.: Tight focusing properties of cylindrically polarized annular multi-Gaussian beam. Optik **127**,7537-7542(2016). doi:10.1016/j.ijleo.2016.05.033 .

65. Li, X., Cao, Y., Tian, N., Fu, L., Gu, M.: Multifocal optical nanoscopy for big data recording at 30 TB capacity and gigabits/second data rate. Optica, **2**(6), 567-570(2015). doi:10.1364/optica.2.000567.
66. Nie, Z. Q., Lin, H., Liu, X.F., et al. Three-dimensional super-resolution longitudinal magnetization spot arrays. Light Sci Appl **6**, e17032(2017) https://doi.org/10.1038/lsa.2017.32.
67. He, K., Wang, X., Wang, Z.W., Yi, H., Scherer, N. F., Katsaggelos, A.K., and Cossairt ,O.: Snapshot multifocal light field microscopy, Opt. Express **28**, 12108-12120(2020). https://doi.org/10.1364/OE.390719.